Magneto-resistance and vortex phase diagram of $BaNi_{0.1}Fe_{1.9}As_2$ single crystal*

Lu Jun-Chao(鲁俊超)[a)†], Yu Yi(于 一)[b)], Pi Li(皮 雳)[c)], and Zhang Yu-Heng(张裕恒)[c)]

[a)] College of Science, Henan University of Technology, Zhengzhou 450001, China
[b)] School of Physics and Material Science, Anhui University, Hefei 230601, China
[c)] High Magnetic Field Laboratory, Chinese Academy of Sciences and University of Science and Technology of China, Hefei 230026, China

(Received 23 April 2014; revised manuscript received 12 June 2014; published online 10 October 2014)

The transition from vortex glass to a liquid phase is studied in $BaNi_{0.1}Fe_{1.9}As_2$ single crystal with $T_c = 19.4$ K by magneto-resistance measurements. The resistivity curves are measured in magnetic fields in a range of 0 T–13 T for $H \parallel c$ and $H \perp c$. Good scalings for all values of resistivity $\rho(H,T)$ and the effective pinning potential $U_0(H,T)$ are obtained with the modified vortex glass theory by using the critical exponents s and H_0. Phase diagrams for $H \parallel c$ and $H \perp c$ are determined based on the obtained vortex glass temperature T_g, the vortex dimensionality crossover temperature T^*, and the upper critical magnetic field H_{c2}. Our results suggest that both below and above 5 T, single vortex pinning co-exists with collective creep, and collective creep is dominant. There is a narrower vortex liquid region for $H \perp c$ than for $H \parallel c$ in the vortex phase diagram, which may originate from a stronger pinning force.

Keywords: Fe-based superconductor, magneto-resistance, pinning, phase transition

PACS: 74.70.Xa, 74.25.Uv, 74.25.Op **DOI:** 10.1088/1674-1056/23/12/127402

1. Introduction

The investigations of magneto-resistance and vortex properties in a mixed state for the iron-based superconductors are crucial to studying their superconducting mechanisms and exploring their potential application aspects. The broadening and tailing of the resistive transition with increasing magnetic field in high-T_c oxypnictide have attracted much attention.[1–6] In the mixed state, thermal fluctuation directly affects the vortex motion by the thermal activated flux flow, leading to the tail at the resistive transition.[6] These features are similar to those of high-T_c superconductors.[7] In contrast to high-T_c superconductors, iron-based superconductors have novel electronic structures.[8] However, the pinning mechanisms and the vortex phase transitions in iron-based superconductors have not been fully understood, especially for the vortex glass phase. According to the vortex glass theory,[9–12] the vortex glass correlation length at the glass transition $T_g(H)$ diverges as $\xi_g(T) = \left|T - T_g\right|^{-\upsilon}$ where ν is the static critical exponent. For a second-order vortex solid–liquid phase transition in highly disordered system, the dc current–voltage (I–V) characteristic for a vortex glass could be scaled onto two or one branches. The experimental results of the I–V curves of the Co-doped Ba-122 single crystal have given a perfect scaling.[11] Therefore, the boundary between the lattice and glass or the glass and liquid phases is strongly affected by both the anisotropy and the disorder of a superconductor. For the Ba-122 system, the anisotropy is only 2–3,[13] so the glass line should be sensitive to dopant and magnetic direction. Vortex phases and magnetic flux pinning mechanisms have been studied in Ba-122 compounds doped by Co, Ni, and K, and so on.[14] However, little work has been reported on the determination of glass lines in iron-based superconductors. Furthermore, most attention has been focused on the results for $H \parallel c$, for the vortex properties for another magnetic field direction are also important.

In this paper, we study the vortex liquid–glass phase transitions in $BaFe_{1.9}Ni_{0.1}As_2$ single crystal by magnetoresistance measurement under $H \parallel c$ and $H \perp c$. We find that the vortex liquid region is narrow for $H \perp c$ compared with for $H \parallel c$, and that all the values of measured resistivity $\rho(H,T)$ in magnetic fields up to 13 T could be scaled. Our results suggest that the vortex glass theory is applicable to describing the vortex glass transition in $BaFe_{1.9}Ni_{0.1}As_2$ single crystal, and the pinning potentials and motion mechanisms are different from their corresponding counterparts in the two applied magnetic field directions.

2. Models

The phase transition can be clearly visualized in resistive behaviors under the magnetic field. According to the vortex glass theory proposed in high T_c cuprate,[11] at the vortex glass transition temperature T_g, the resistivity varies as a power law

$$\rho = \rho_0 \left| \frac{T}{T_g} - 1 \right|^s, \quad (1)$$

*Project supported by the Foundation of Henan Educational Committee, China (Grant No. 13B140951) and the Foundation of Henan University of Technology, China (Grant Nos. 11JCYJ15 and 2011BS030).

†Corresponding author. E-mail: jchlu@mail.ustc.edu.cn

© 2014 Chinese Physical Society and IOP Publishing Ltd

where ρ_0 is a characteristic resistivity in normal state, s is a constant related to the type of disorder. At the glass line, equation (1) should be modified as[15]

$$\rho = \rho_n \left| \frac{k_B T}{U_0(H,T)} - 1 \right|^s, \tag{2}$$

where U_0 is the pinning potential, k_B is the Boltzmann constant, and ρ_n is the resistivity in a normal state. To extract the relation between the explicit field and temperature, the $U_0(H,T)$ could be expressed as[16]

$$U_0(H,T) = k_B T_c \frac{1-t}{(H/H_0)^\beta}, \tag{3}$$

where $t = T/T_c$, B_0 and β are field- and temperature-independent constants respectively. In the thermal activation model, the resistance can be considered to be a result of the competition between thermal activation $k_B T$ and the effective pinning energy. Combining Eqs. (2) and (3), one obtains a typical scaling function for resistivity

$$\rho = \rho_n \left| \frac{T(T_c - T_g)}{T_g(T_c - T)} - 1 \right|^s. \tag{4}$$

3. Experimental details

The Ni-doped $BaNi_{0.1}Fe_{1.9}As_2$ single crystals were grown by self-flux method.[17] The dimensions of the sample were 1.18 mm × 1.25 mm × 0.34 mm. The sample has a T_c of 19.4 K and a small superconducting transition width (10%–90%) of 0.6±0.1 K. Temperature-dependent electrical resistivity was measured by using a Quantum Design Physical Property Measurement System. The electrical contacts were placed on samples in standard 4-probe geometry, and the current flowed within *ab*-plane. The resistivity values were measured in the *ab*-plane (ρ_{ab}) and *c*-direction (ρ_c) for $BaNi_{0.1}Fe_{1.9}As_2$ single crystal over a wide temperature range at magnetic fields in a range of 0 T–13 T.

4. Results and discussion

When the applied current is small, the pinning barriers are large compared with the thermal energy, but are still finite. In this case, the vortex system acts as a very viscous liquid. According to the thermal assistant flux flow (TAFF) model,[18] one obtains an Ohmic resistivity

$$\rho = \rho_0 e^{-U_0/\kappa_B T}, \tag{5}$$

where U_0 is the pinning potential which is both field- and temperature-dependent. Equation (2) suggests that the resistivity in the TAFF regime will show linear behavior in the Arrhenius plot of $\ln\rho$ versus $1/T$. Figures 1(a) and 1(b) show the variations of resistance $R(H,T)$ with $1/T$ of $BaNi_{0.1}Fe_{1.9}As_2$ single crystal near the superconducting transition for $H \parallel c$ and $H \perp c$ axis, respectively. Note that the results are shown in a common logarithmic scale. By increasing the magnetic fields, the resistivity transition widths are broadened gradually. The superconductivity values shift toward lower temperatures for both magnetic field directions, but the trend is more obvious for $H \parallel c$ than for $H \perp c$. In the TAFF region, the curves all show Arrhenius relations.

According to the vortex glass model,[9] resistance varies at the vortex glass temperature T_g as $\rho \propto |T - T_g|^s$, $s = \nu(1-z)$, where ν is a static exponent related to the vortex glass correlation length, $\xi_g \sim (T - T_g)^{-\nu}$, and z is a dynamic exponent for the correlation time, $T_g \sim \xi_g^z$. Therefore, the Vogel–Fulcher relation $[d(\ln\rho)/dT]^{-1}$ is usually used to analyze the vortex glass boundary. According to Eq. (4), the inverse of the logarithmic derivative of the resistivity will be linearly dependent on T as

$$\left[\frac{d(\ln\rho)}{dt}\right]^{-1} = \frac{1}{s}(T - T_g). \tag{6}$$

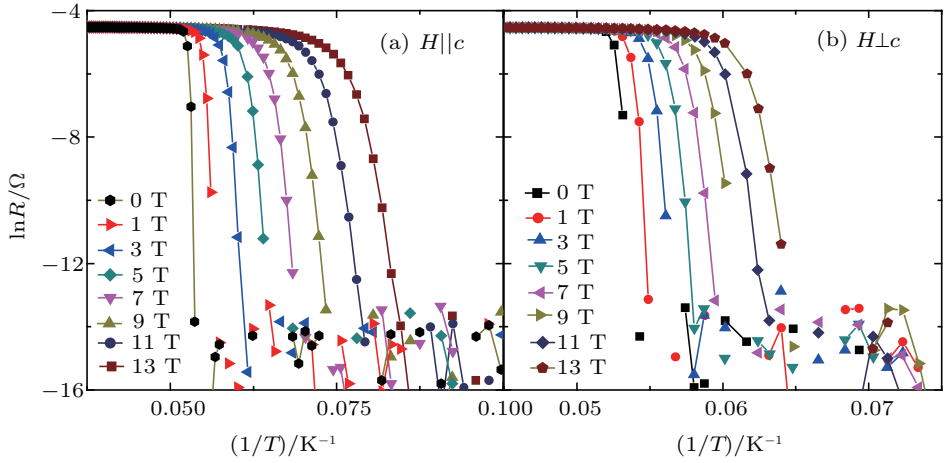


Fig. 1. (color online) Arrhenius plots of the resistance for $BaNi_{0.1}Fe_{1.9}As_2$ single crystal for (a) $H \parallel c$ and (b) $H \perp c$. The applied magnetic fields are (from left to right) 0, 1, 3, 5, 7,9, 11, and 13 T.

Figure 2 shows the temperature dependence of $[\mathrm{d}(\ln\rho)/\mathrm{d}T]^{-1}$ under various magnetic fields of 1 T–13 T for $H \parallel c$ and $H \perp c$. By fitting the linear region of the curves according to Eq. (6), T_g and T^* are estimated. T^* is a critical temperature, at which the curve deviates from linearity, corresponding to the upper temperature limit of the critical region associated with the transition from vortex glass to vortex liquid.[6] As we can see in Fig. 2, the resistances of $BaNi_{0.1}Fe_{1.9}As_2$ are well described by the vortex-glass picture in a temperature range of $T_g < T < T^*$. The temperature-dependent resistances have also been investigated for other pnictides such as $SmFeAsO_{0.85}$[19] and (Ba, K)Fe_2As_2.[20] The values of exponent s and the slop of the fitting straight line are obtained as 2.7±0.2 and 1.5±0.3 for $H \parallel c$ and $H \perp c$, respectively. The value of s for $H \parallel c$ is consistent with the corresponding results of (Ba, K)Fe_2As_2.

Equation (4) suggests a scaling behavior in the double logarithmic plot of ρ versus T. According to Eq. (4), the resistive curves for different fields should scale into one when the normalized resistivity ρ/ρ_n is plotted versus scaled temperature $T_{sc} = [T(T_c - T_g)/(T_c - T) - 1]$. Figure 3 shows the ρ/ρ_n dependences on scaling temperature T_{sc} for different magnetic field directions, respectively. The combined exponents s and T_g are obtained from the inverse of the slop and the intersection with the temperature axis of the linear parts of these curves in Fig. 3. As can be seen in Fig. 3, all the resistivity transitions between 0 T and 13 T are scaled into one curve with the obtained critical exponents. These scaled results are similiar to the behaviors observed in high-T_c cuprates such as Y-123[21,22] and BSCCO[23] single crystals, Tl-2212 thin films,[24] etc.

According to Eq. (2), the pinning energy U_0 could be obtained as

$$U_0(T,B) = k_B T \left[1 + \left(\frac{\rho}{\rho_n}\right)^{1/s}\right]^{-1}. \quad (7)$$

Therefore, both the field- and temperature-dependent U_0 could be obtained from the experimental data, provided that the ρ_n and s are known. s is estimated as mentioned above and ρ_n is resistivity in a normal state. The calculated values of U_0 at magnetic fields between 0 T and 13 T are shown in Figs. 4(a) and 4(b) for $H \parallel c$ and $H \perp c$, respectively.

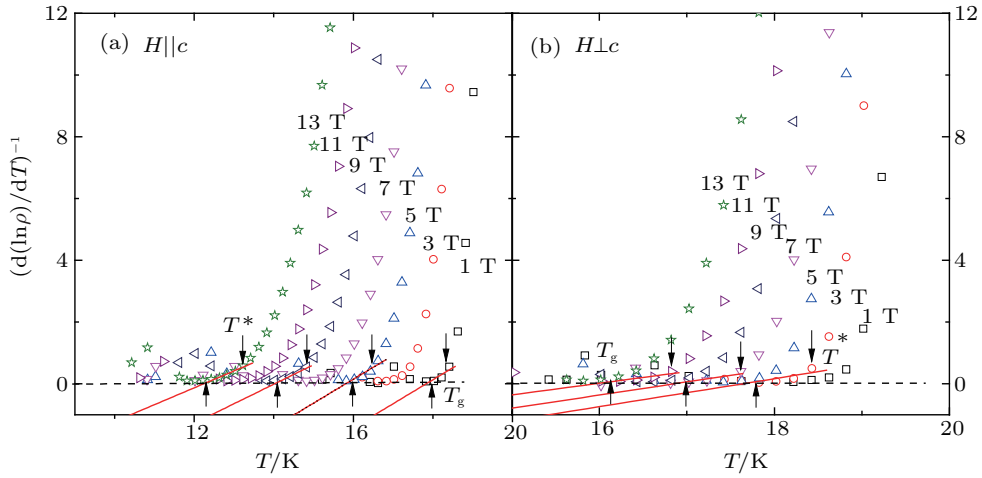


Fig. 2. (color online) Temperature dependences of $[\mathrm{d}(\ln\rho)/\mathrm{d}T]^{-1}$ data at magnetic fields H = 1, 3, 5, 7, 9, 11, and 13 T for (a) $H \parallel c$ and (b)$H \perp c$. The vortex glass temperature T_g and a critical temperature T^* are estimated according to the linear fitting. The solid lines denote linear fittings to Eq. (6), and the dashed line represents the position of the original point of the vertical axis.

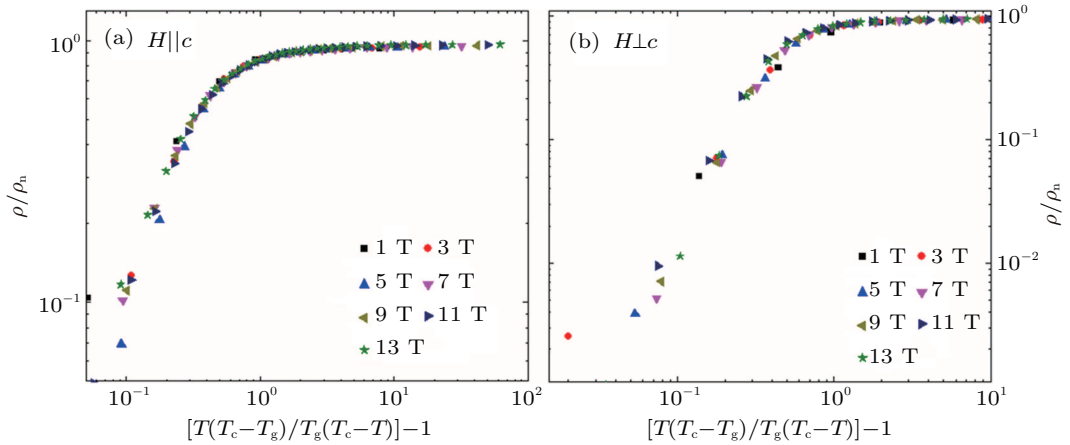


Fig. 3. (color online) Scalings of the temperature-dependent resistivity according to Eq. (4) under the magnetic fields of 0 T–13 T for $BaNi_{0.1}Fe_{1.9}As_2$ single crystal in the cases of (a) $H \parallel c$, (b) $H \perp c$.

The solid lines represent the linear fittings to Eq. (3). As can be seen in Fig. 4, the curves at low magnetic fields (less than 11 T) are very well consistent with Eq. (3). According to Eq. (3), we have $U_0\ (T_c) = 0$ at the critical transition temperature T_c, and at the vortex glass temperature T_g we have $U_0\ (T_g) = k_B T_g$. Therefore, the field-dependent part $U_B = k_B T_c/(H/H_0)^{\beta}$ could be directly obtained from the slope of the fitting lines. The results are shown in Fig. 5. As we can see in Fig. 5, the pinning potential for $H \perp c$ is higher than for $H \parallel c$. This is an obvious result. As is well known, the pancake vortices in *ab* planes are pinned by Josephson coupling between superconducting planes, while the Josephson vortices are pinned by normal layers. The U_B/k_B shows different dependences of magnetic fields for $H < 5$ T and $H > 5$ T. For $H < 5$ T and $H > 5$ T, the U_B/k_B values decrease respectively as $B^{-0.4}$ and $B^{-0.8}$ for $H \perp c$, while scale respectively as $B^{-0.6}$ and $B^{-1.0}$ for $H \parallel c$. The result suggests different pinning mechanisms for low and high magnetic fields. The weak field dependences of $U_B(H)/k_B$ in the low field for both orientations indicate that single-vortex pinning dominates in this region.[25] The vortex spacing becomes significantly smaller than the penetration depth in higher fields and a crossover in a collective-pining regime where the activation energy becomes strongly dependent on the field, i.e. the collective creep is dominant.[26] Similar crossovers were also observed in Nd(O, F)FeAs[27] and Fe_{1+y} $(Te_{1-x}, S_x)_z$ single crystals.[28]

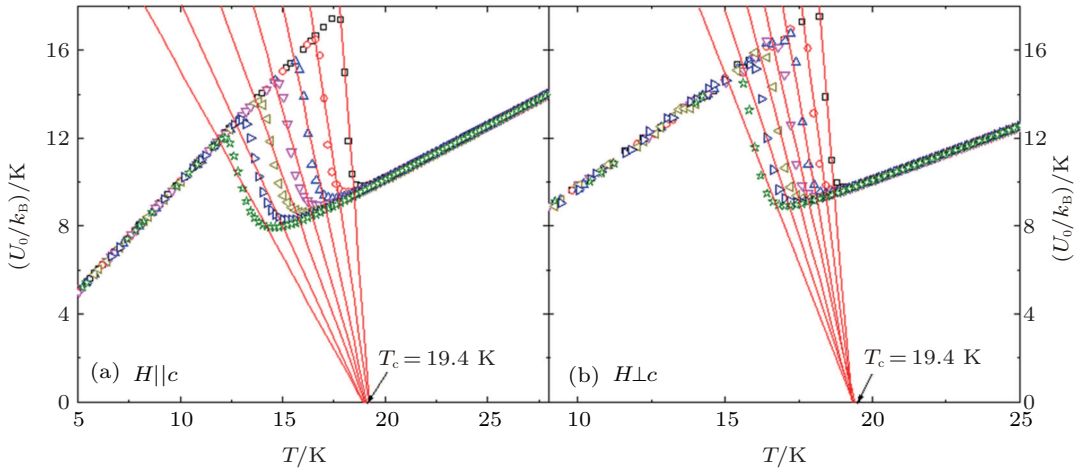


Fig. 4. (color online) Calculated pinning potential $U_0(H,T)$ values according to Eq. (7) for $BaNi_{0.1}Fe_{1.9}As_2$ single crystal in the cases of (a) $H \parallel c$; (b) $H \perp c$. The solid lines denote linear fittings to Eq. (3). All the fitting lines intersect at about $T_c = 19.4$ K.

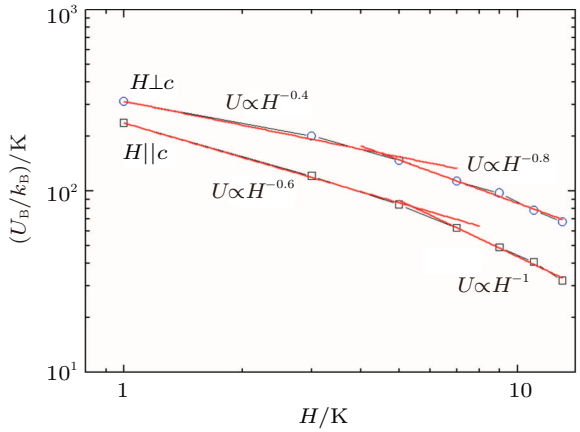


Fig. 5. (color online) Magnetic field dependences of U_B/k_B estimated from Eq. (3) and the slopes in Fig. 4. The solid lines denote the fittings to the data, giving the relation $U_B/k_B \propto H^{-0.6}$ for $H < 5$ T and $U_B/k_B \propto H^{-1}$ for $H > 5$ T for $H \parallel c$ (empty squares). For $H \perp c$ (empty circles), the fittings to the data, giving different relation $U_B/k_B \propto H^{-0.4}$ for $H < 5$ T and $U_B/k_B \propto H^{-0.8}$ for $H > 5$ T.

Finally, combining the experimental results above, the obtained vortex phase diagrams for $BaNi_{0.1}Fe_{1.9}As_2$ single crystal with different dynamic characteristics are shown in Fig. 6. The upper critical field, H_{c2}, is obtained from the 90% value of its corresponding resistivity transition, and the vortex glass line H_g and the upper field limit of the critical region associated with the vortex glass to liquid phase transition, H^*, are estimated from Fig. 2. The H^* lines are obtained as follows: First, we could estimate T^* values for 1 T–13 T from Figs. 2(a) and 2(b), where T^* is the temperature which deviates from linearity. Then, we plot H_g, H^*, and H_{c2} in the H–t $(t = T/T_c)$ phase diagrams for the cases of $H \parallel c$ and $H \perp c$ as shown in Fig. 6. As usually observed in high T_c cuprats, a transition from vortex glass to a liquid phase is found in our $BaNi_{0.1}Fe_{1.9}As_2$ single crystal below H_{c2}. At magnetic fields $H > H_g$. The vortex lattice becomes softer and eventually melts via a first-order transition into the vortex liquid.[29] At H^*, the vortex system undergoes a dimensionality transition from 2D to 3D, and above H_{c2}, the system enters into normal state. As can be seen in Fig. 6, the vortex liquid region is narrower for $H \perp c$ than for $H \parallel c$, which originates from stronger pinning for $H \perp c$.

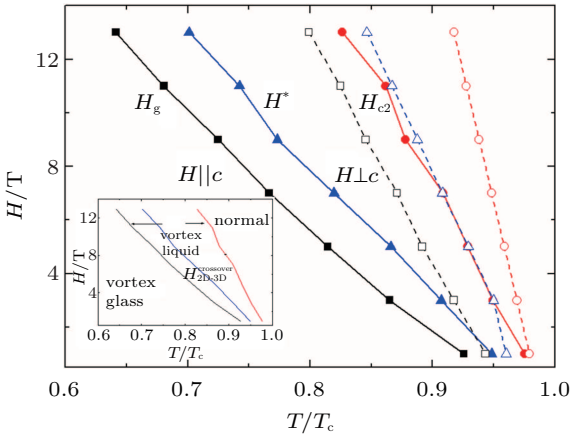


Fig. 6. (color online) Static vortex phase diagram of $BaNi_{0.1}Fe_{1.9}As_2$ for $H \parallel c$ (solid symbols) and $H \perp c$ (open symbols). The upper critical magnetic fields H_{c2} are estimated from the criterion of the 90% values of their corresponding resistivity transition. The characteristic field H_g for vortex glass-to-liquid transition, and 2D–3D crossover fields H^* are determined from Fig. 2.

5. Conclusion

In this paper, we analyze the resistivity transitions and vortex phase transitions of a $BaNi_{0.1}Fe_{1.9}As_2$ single crystal for $H \parallel c$ and $H \perp c$. For temperatures below superconductive temperature T_c, scalings of all measured values of resistivity $\rho(H,T)$ in magnetic fields up to 13 T with the values of critical component s are obtained. The vortex phase diagrams and pinning potential $U_0(H,T)$ values for $H \parallel c$ and $H \perp c$ are determined based on the obtained vortex glass lines and upper critical magnetic field B_{c2} values. The results suggest a narrower vortex liquid region for $H \perp c$, corresponding to a stronger pinning force. For low and high magnetic fields, the dependences of $U_0(H,T)$ on B are different due to different pinning mechanisms.

References

[1] Maiorov B, Katase T, Baily S A, Hiramatsu H, Holesinger T G, Hosono H and Civale L 2011 *Supercond. Sci. Technol.* **24** 055007

[2] Tarantini C, Lee S, Zhang Y, Jiang J, Bark C W, Weiss J D, Polyanskii A, Nelson C T, Jang H W, Folkman C M, Baek S H, Pan X Q, Gurevich A, Hellstrom E E, Eom C B and Larbalestier D C 2010 *Appl. Phys. Lett.* **96** 142510

[3] Shahbazi M, Wang X L, Lin Z W, Zhu J G, Dou S X and Choi K Y 2011 *J. Appl. Phys.* **109** 07E151.

[4] Sun D L, Liu Y and Lin C T 2009 *Phys. Rev. B* **80** 144515.

[5] Pramanik A K, Harnagea L, Singh S, Aswartham S, Behr G, Wurmeh S, Hess C, Klingeler R and Büchner B 2010 *Phys. Rev. B* **82** 014503.

[6] Song Y J, Kang B, Rhee J S and Kwon Y S 2012 *Europhys. Lett.* **97** 47003

[7] Liu S L, Wu G, Xu X B, Wu J and Shao H M 2005 *Supercond. Sci. Technol.* **18** 1332

[8] Huang Y B, Richard P, Wang J H, Wang X P, Shi X, Xu N, Wu Z, Li A, Yin J X, Qian T, LV B, Chu C W, Pan S H, Shi M and Ding H 2013 *Chin. Phys. Lett.* **30** 17402

[9] Fisher M P A 1989 *Phys. Rev. Lett.* **62** 1415

[10] Koch R H, Foglietti V, Gallagher W J, Koren G, Gupta A and Fisher M P A 1989 *Phys. Rev. Lett.* **63** 1511

[11] Fisher D S, Fisher M P A and Huse D A 1991 *Phys. Rev. B* **43** 130

[12] Tamegai T, Taniguchi T, Taen T, Nakajima Y, Nishizaki T, Naito T, Kobayashi N, Kitamura H and Murakami T 2012 *26th International Conference on Low Temperature Physics, J. Phys.: Conference Series* **400** 022122

[13] Yamamoto A, Balicas L, Jaroszynski J., Tarantini C, Jiang J, Gurevich A, Larbalestier D C, Jin R, Sefat A S, McGuire M A, Sales B C, Christen D K and Mandrus D 2009 *Appl. Phys. Lett.* **94** 062511

[14] Ghorbani S R, Wang X L, Shabazi M, Dou S X, Choi K Y and Lin C T 2012 *Appl. Phys. Lett.* **100** 072603

[15] Rydh A, Rapp Ö, and Andersson M 1999 *Phys. Rev. Lett.* **83** 1850

[16] Wen H H, Radovan H A, Kamm F M, Ziemann P, Yan S L, Fang L and Si M S 1998 *Phys. Rev. Lett.* **80** 3859

[17] Wang M Y, Luo H Q, Zhao J, Zhang C L, Wang M, Marty K, Chi S X, Lynn J, Schneidewind A, Li S L and Dai P C 2010 *Phys. Rev. B* **81** 174524

[18] Kes P, Aarts J, van den Berg J, van der Beek C and Mydosh J 1989 *Supercond. Sci. Technol.* **1** 242

[19] Lee H S, Bartkowiak M, Kim J S and Lee H J 2010 *Phys. Rev. B* **82** 104523

[20] Kim H J, Liu Y, Oh Y S, Khim S H, Kim I, Stewart G R and Kim K H 2009 *Phys. Rev. B* **79** 014514

[21] Rydh A, Rapp Ö and Andersson M 1999 *Phys. Rev. Lett.* **83** 1850

[22] Andersson M, Rydh A and Rapp Ö 2001 *Phys. Rev. B* **63** 184511

[23] Minnhagen P 1989 *Solid State Commun.* **71** 25

[24] Arronte B E and Andersson M 2005 *Phys. Rev. B* **71** 024507

[25] Blatter G, Feigel'man M V, Geshkenbein V B, Larkin A I and Vinokur V M 1994 *Rev. Mod. Phys.* **66** 1125

[26] Yeshurun Y and Malozemoff A P 1988 *Phys. Rev. Lett.* **60** 2202

[27] Jaroszynski J, Hunte F, Balicas L, Jo Y J, Raičević I, Gurevich A, Larbalestier D C, Balakirev F, Fang L, Cheng P, Jia Y and Wen H H 2008 *Phys. Rev. B* **78** 174523

[28] Lei H C, Hu R W, Choi E S and Petrovic C 2010 *Phys. Rev. B* **82** 134525

[29] Rosenstein B and Li D P 2010 *Rev. Mod. Phys.* **82** 109